Carbon 185 (2021) 282–288

Contents lists available at ScienceDirect

Carbon

journal homepage: www.elsevier.com/locate/carbon

Research Paper

Intrinsic phonon anharmonicity in heavily doped graphene probed by Raman spectroscopy

X. Chen [a, b], M.-L. Lin [a], X. Cong [a, b], Y.-C. Leng [a, b], X. Zhang [a], P.-H. Tan [a, b, *]

[a] State Key Laboratory of Superlattices and Microstructures, Institute of Semiconductors, Chinese Academy of Sciences, Beijing, 100083, China
[b] Center of Materials Science and Optoelectronics Engineering & CAS Center of Excellence in Topological Quantum Computation, University of Chinese Academy of Sciences, Beijing, 100049, China

ARTICLE INFO

Article history:
Received 6 July 2021
Received in revised form
7 September 2021
Accepted 8 September 2021
Available online 18 September 2021

Keywords:
Heavily-doped graphene
Phonon anharmonicity
Electron-phonon coupling
Temperature dependent Raman spectroscopy
$FeCl_3$-based stage-1 graphite intercalation compound

ABSTRACT

The temperature-dependent (*T*-dependent) linewidth (Γ_G) and frequency shift ($\Delta\omega_G$) of the G mode provide valuable information on the phonon anharmonicity of graphene-based materials. In contrast to the negligible contribution from electron-phonon coupling (EPC) to the linewidth of a Raman mode in semiconductors, Γ_G in pristine graphene is dominated by EPC contribution at room temperature due to its semimetallic characteristics. This leads to difficulty in resolving intrinsic contribution from phonon anharmonicity to Γ_G. Here, we probed the intrinsic phonon anharmonicity of heavily-doped graphene by *T*-dependent Raman spectra based on $FeCl_3$-based stage-1 graphite intercalation compound (GIC), in which the EPC contribution is negligible due to the large Fermi level (E_F) shift. The $\Delta\omega_G$ and Γ_G exhibit a nonlinear decrease and noticeable broadening with increasing temperature, respectively, which are both dominated by phonon anharmonicity processes. The contribution of phonon anharmonicity to Γ_G of heavily-doped graphene decreases as the E_F approaches to the Dirac point. However, the *T* dependence of $\Delta\omega_G$ is almost independent on E_F and qualitatively agrees with the theoretical result of pristine graphene. These results provide a deeper understanding of the role of phonon anharmonicity on the Raman spectra of heavily doped graphene.

1. Introduction

Graphene, a planar single sheet of sp^2-bonded carbon atoms arranged in honeycomb lattice, has attracted extensive attention owing to its unique properties, such as excellent thermal conductivity [1,2]. Thermal transport in pristine graphene can be described properly only if both the phonon scattering process and electron-phonon coupling (EPC) are taken into account because of its gapless feature [3]. Consequently, a comprehensive understanding of these processes that determine the thermal transport property of graphene is key for the design of efficient graphene-based nanoelectronic devices.

Temperature-dependent (*T*-dependent) full width at half maximum (FWHM) and peak position of the G mode can provide powerful information on the phonon anharmonicity and EPC of graphene-based materials, which are easily accessible by Raman scattering technique [4–7]. In general, the FWHM of the G mode (Γ_G) in the Raman spectrum of graphene-based materials includes the contributions from phonon-phonon (ph-ph) term (Γ_G^{an}) and EPC term (Γ_G^{EPC}) [8], which are, respectively, determined by the anharmonic terms in the interatomic potential [9,10] and EPC strength [11]. The Γ_G^{an} term always exists, while the Γ_G^{EPC} term is only present in graphene-based materials when their Fermi energy (E_F) is comparable or smaller than half of the G mode energy. At room temperature, EPC contribution in pristine graphene dominates Γ_G, and it is significantly sensitive to its E_F [7,8,12–14]. As graphene can be easily doped by carrier transfer from donnors/acceptors, it is difficult to distinguish Γ_G^{an} from Γ_G^{EPC} in Γ_G. For example, Lin et al. [6] and Nguyen et al. [14] found that Γ_G^{an} is ~ 8.5 cm^{-1} at 0 K in vertical graphene sheets and ~ 9.2 cm^{-1} at 296 K in as-exfoliated graphene on SiO_2/Si substrate, respectively. However, Efthimiopoulos et al. [15] reported that Γ_G^{an} is ~ 4.9 cm^{-1} at 0 K in graphene nanoplatelets. In graphite, Liu et al. [7] reported that Γ_G^{an} can be as small as ~ 1.6 cm^{-1} at 0 K. In spite of the above fact,

* Corresponding author. State Key Laboratory of Superlattices and Microstructures, Institute of Semiconductors, Chinese Academy of Sciences, Beijing, 100083, China.
E-mail address: phtan@semi.ac.cn (P.-H. Tan).

https://doi.org/10.1016/j.carbon.2021.09.017
0008-6223/

most of the T-dependent Γ_G of as-prepared graphene flakes and graphite are fitted by both Γ_G^{an} and Γ_G^{EPC} terms [3,6,7,15–17] with varied $\Gamma_G^{EPC}(T = 0\ K)$ from 9.1 to 12 cm^{-1}. However, individual Γ_G^{EPC} had ever been used to fit the corresponding T-dependent Raman spectra measured in graphene electrostatically gated near the charge neutrality point [14], and the corresponding $\Gamma_G^{EPC}(T = 0\ K)$ was as large as ~ 21.5 cm^{-1}. These results show that there exists apparent inconsistency for both Γ_G^{an} and Γ_G^{EPC} contributions in graphene flakes and graphite between experiments from different groups [3,6,7,14–17]. Thus, it is difficult to directly probe intrinsic ph-ph contribution in pristine graphene by Raman spectroscopy. In contrast, if graphene is heavily doped, and its $|E_F|$ is larger than half of the G mode energy, the EPC contribution can be neglected due to the Pauli exclusion principle. In this case, T-dependent Γ_G ($\Gamma_G(T)$) in heavily-doped graphene can present a direct signature of intrinsic ph-ph contribution to Γ_G in graphene, which is essential to be explored in experiments.

In general, graphene can be heavily doped by chemical doping, electrochemical doping, or electrostatic backgating through a substrate [13,18–20]. Due to the wide variation of intercalants, chemical doping of graphite by intercalation was commonly used to obtain graphite intercalation compounds (GICs) [21]. GICs show distinct physical properties, including different electrical, thermal and magnetic characteristics [21–24]. Anhydrous ferric chloride ($FeCl_3$) is often used to prepare acceptor-type GICs [19,21]. $FeCl_3$-based stage-1 GICs are very stable in air, whose adjacent graphene layers are isolated by $FeCl_3$ layer, leading to layer-by-layer decoupling. The charge transfer between $FeCl_3$ and the neighboring graphene layers induces high doping level in graphene layers [19,25]. Owning to the decoupling and charge transfer, $FeCl_3$-based stage-1 GIC can be treated as heavily-doped individual graphene layers. Indeed, the electronic properties of stage-1 GIC behave like graphene, *e.g.*, linear dispersion near the Dirac point [23,25], and its 2D band exhibits a single Lorentzian line shape [19,23–25], showing typical spectral feature of graphene. Graphene layers in stage-1 GICs with different E_F can be archived by controlling the dose of $FeCl_3$ intercalants. Therefore, $FeCl_3$-based GIC provides an ideal platform for investigating the phonon anharmonicity effect in heavily-doped graphene.

In this work, we have performed T-dependent Raman experiments on four heavily-doped graphene flakes of $FeCl_3$-based stage-1 GICs with different E_F. The experimental frequency shift of the G mode with temperature are independent on E_F, and are in line with the theoretical results by density functional theory calculations. The Pauli blocking near K(K′) point of heavily-doped graphene prevents phonon from decaying into electron-hole pairs, thus the intrinsic ph-ph contribution to $\Gamma_G(T)$ is measured, which is much larger than that of pristine graphene.

2. Experimental methods

GIC Fabrication: Pristine monolayer graphene and graphite flakes were obtained by micromechanical cleavage of natural graphite onto the surface of a Si wafer chip, covered with 90-nm-thick SiO_2 on the top [26]. Intercalation of graphite flakes by $FeCl_3$ was prepared following the vapor transport method commonly used for GICs [19]. Firstly, the intercalant $FeCl_3$ and graphite flakes were positioned in different zones in a glass tube. Next, in order to ensure that $FeCl_3$ is anhydrous, the glass tube was pumped to ~1.5×10^{-4} Torr and kept at 393 K for more than half an hour. Then, it was sealed and inserted into an oven with a reaction temperature of 613 K for 30 h to synthesize $FeCl_3$-based stage-1 GICs. Finally, they were immediately removed from the still hot glass tube because GICs are more stable in air than in vacuum [19].

T-dependent Raman measurements: A helium cooled cryogenic station (Montana Instruments) and THMS350V (Linkam Scientific Instruments) were used for T-dependent Raman measurements in the ranges of 4~300 K and 77~500 K, respectively. The measurements were carried out in back-scattering geometry using a Jobin-Yvon HR800 system equipped with a liquid nitrogen cooled charge-coupled detector. The excitation wavelengths are 632.8 nm from a He-Ne laser and 514.5 nm from an Ar^+ laser. An 1800 lines/mm grating is used to achieve a spectral resolution of 0.45 cm^{-1} at around 632.8 nm. For all the measurements, laser power was kept below 1 mW to avoid sample heating. The spectral broadening of the Raman system is ~ 1.0 cm^{-1} by estimating from the Rayleigh signal at 0.0 cm^{-1}.

3. Results and discussions

Fig. 1(a) shows the optical images of four $FeCl_3$-based GIC flakes, which are marked as S1, S2, S3, and S4, respectively. Their Raman spectra in Fig. 1(b) excited by 514.5 nm exhibit prominent G and 2D modes whose frequencies are close to the G and 2D modes in pristine graphene, respectively. The absence of the D mode in these four GIC flakes implies defects free of the samples. The line shape of the 2D mode is often used to identify the number of layers of graphene flakes [27]. The 2D band of all the four GIC flakes exhibits a single Lorentzian lineshape, other than multiple Lorentzian peaks of multilayer graphene or graphite flakes, demonstrating the electronic decoupling of the adjacent graphene layers in graphite flakes after intercalation by $FeCl_3$ [19]. This suggests that the four GIC flakes are stage-1 GICs [19,21,28], in which each graphene layer is sandwiched by $FeCl_3$ layers, as shown in Fig. 1(c). In $FeCl_3$-based stage-1 GICs, the electrons in graphene layer are transferred to the adjacent $FeCl_3$ layers, resulting in its hole doping [19,21]. This can be confirmed by the blue shift of the 2D band in S1–S4 (Fig. 1(b)) relative to that in pristine graphene [27,29].

Both the Raman intensity ratio of the 2D mode to the G mode (I(2D)/I(G)) and the peak position of the G mode (ω_G) are very sensitive to the doping level of graphene [30]. The higher the doping level is, the larger ω_G and the smaller I(2D)/I(G) can be observed. Indeed, I(2D)/I(G) is smaller than that in pristine graphene and gradually decreases from S1 to S4. In comparison to ω_G at 1582 cm^{-1} in pristine graphene, ω_G of S1, S2, S3 and S4 significantly blueshifts and, respectively, locates at 1605, 1611, 1619 and 1626 cm^{-1}. These results indicate that the four GIC flakes exhibit different E_F. The shift of E_F has two major effects on the ω_G of graphene: (1) a change of the equilibrium lattice parameter [29,31,32], and (2) the onset of effects beyond the adiabatic Born-Oppenheimer approximation [8,12,33]. The second effect always results in a G mode blueshift [12,13], while the first one leads to a blueshift of the G mode only for p doping [29,32]. As reported by previous works [8,12], E_F of graphene is approximately linear to ω_G as $|E_F| = \delta\omega_G/42$, where $\delta\omega_G$ is the frequency shift of the G mode in doped graphene relative to that in pristine graphene [34]. According to ω_G of pristine graphene at 1582 cm^{-1}, we can estimate E_F of S1, S2, S3 and S4 as −0.55 eV, −0.69 eV, −0.88 eV and −1.05 eV, respectively. The estimated E_F of −1.05 eV in S4 is close to that (~−0.9 eV) of the corresponding GIC flake determined by multi-wavelength excited Raman spectroscopy [19]. Obviously, these stage-1 GIC flakes are heavily doped with high doping level and can be used as prototypes to study physical properties of heavily-doped graphene, *e.g.*, the contribution of phonon anharmonicity and EPC to its T-dependent Raman spectrum. In heavily-doped graphene with $|E_F|$ larger than $\frac{1}{2}\hbar\omega_G$, the electronic transitions within $2|E_F|$ at K(K′) point are forbidden due to the Pauli exclusion principle [8,12,19], as shown in Fig. 1(d), and the decay channel of phonons

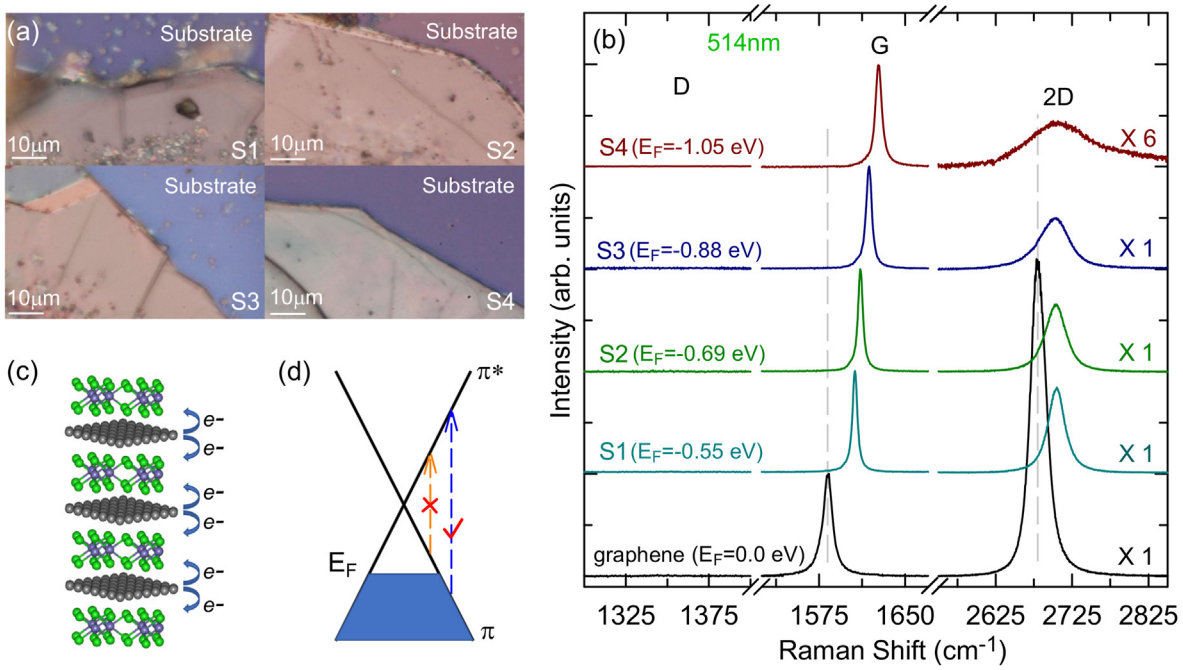

Fig. 1. (a) Optical images of four stage-1 GIC flakes, S1–S4. The scale bar is 10 μm. (b) Raman spectra of pristine graphene and S1–S4 excited by 514.5 nm at room temperature, E_F of each flake is indicated. All spectra are normalized by I(G). (c) Schematic illustration of a stage-1 GIC, where Cl, Fe and C atoms are color coded in green, purple, and dark-gray, respectively. (d) Schematic diagram of hole-doped graphene with E_F, where the electronic transition with energy below $2E_F$ is forbidden. (A colour version of this figure can be viewed online.)

into electron-hole pairs is also blocked. In this case, T-dependent Raman spectrum of heavily-doped graphene should be significantly distinct from that of pristine graphene or graphite.

Fig. 2 presents contour plots of T-dependent G mode in heavily-doped graphene (S1–S4) excited by 632.8 nm and graphite (as a reference sample) excited by 514.5 nm in the temperature range of 4~500 K. For graphite, with increasing T, its $\omega_G(T)$ exhibits redshift while its $\Gamma_G(T)$ becomes slightly narrow, as reported in the previous work [7]. For S1–S4, with increasing T, their $\omega_G(T)$ also exhibits similar redshift as that of graphite; however, their $\Gamma_G(T)$ is much smaller than that of graphite and exhibits significant broadening. With the increase of E_F, the broadening of $\Gamma_G(T)$ becomes more obvious at higher T.

The frequency shift of $\omega_G(T)$ in graphene relative to that at ~0 K, *i.e.*, $\Delta\omega_G(T)$, results from its phonon anharmonicity and thermal expansion (TE). The experimental data of $\Delta\omega_G(T)$ in graphite [7] and S1–S4 excited by 632.8 nm are summarized by diamonds in Fig. 3. The T-dependent Raman behaviors of S2–S4 are further confirmed by Raman spectra excited by 514.5 nm in the range of 4~300 K, as depicted by open circles in Fig. 3. This is also true for graphite [7]. Previous reports in graphite and graphene observed a linear dependence of $\Delta\omega_G$ on temperature [5,14,35]. However, $\Delta\omega_G$ of S1–S4 exhibits similar non-linear T dependence, more significant than that of graphite [7].

Considering the contribution from TE term ($\Delta\omega^{TE}(T)$) and anharmonic ph-ph interaction ($\Delta\omega^{an}(T)$), the T-dependent frequency shift of a Raman-active mode can be simply described by Ref. [7]:

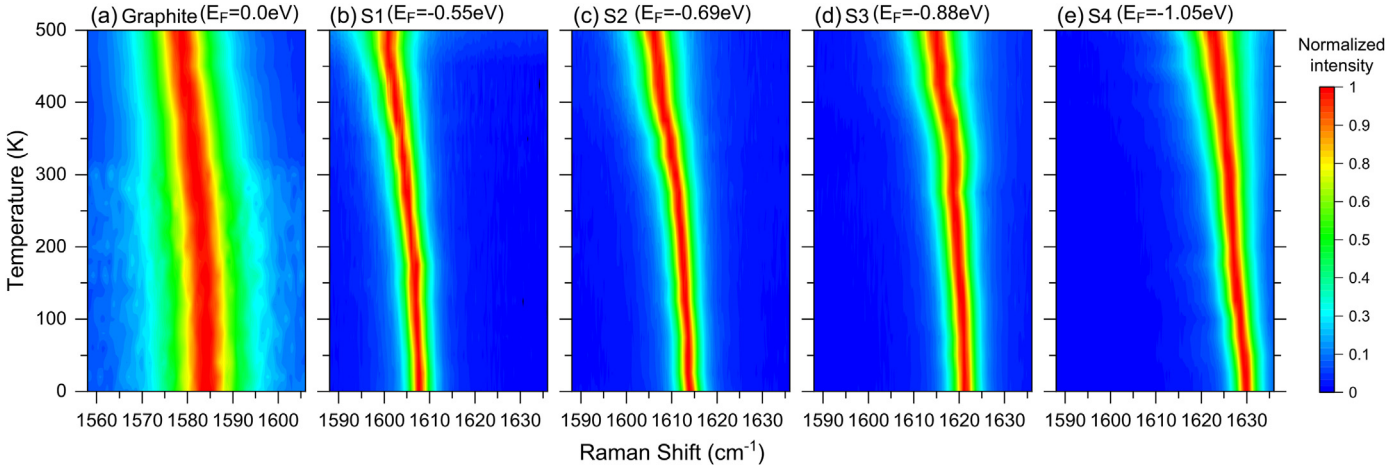

Fig. 2. Contour plots of T-dependent G mode in (a) graphite (reference sample) excited by 514.5 nm [7] and (b–e) S1–S4 excited by 632.8 nm in the temperature range of 4 ~500 K. Notably, I(G) of each spectrum is normalized to 1 for the sake of FWHM comparison. (A colour version of this figure can be viewed online.)

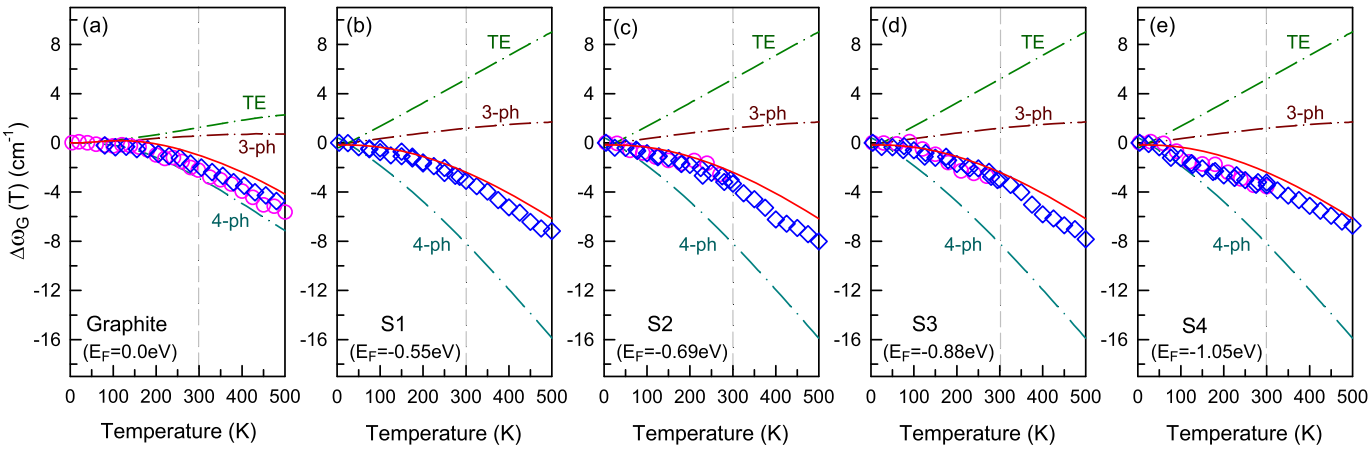

Fig. 3. *T*-dependent $\Delta\omega_G$ of (a) graphite [7] and (b–e) S1–S4 excited by 632.8 nm (blue open diamonds) and 514.5 nm (pink open circles). The solid lines indicate the theoretical results [36] of $\Delta\omega_G$ in graphite (a) and pristine graphene (b–e), including the contributions from TE, 3-ph and 4-ph terms (dash-dotted lines as labelled). Vertical gray dashed lines are guides to the eye at room temperature. (A colour version of this figure can be viewed online.)

$$\Delta\omega(T) = \omega(T) - \omega(0) = \Delta\omega^{TE}(T) + \Delta\omega^{an}(T), \quad (1)$$

where $\omega(0)$ is the frequency of the Raman mode at ~ 0 K. TE contribution originates from the change of volume with temperature by the following equation [37,38]:

$$\Delta\omega^{TE}(T) = \omega(0)\exp\left[-\eta\gamma_G\int_0^T \alpha(T')\,dT'\right], \quad (2)$$

where γ_G is the Grüneisen constant, $\alpha(T)$ denotes the linear *T*-dependent expansion coefficient of the material, η represents the dimensionality factor of the material and $\eta = 2$ for the G mode in graphene and graphite. On the other hand, $\Delta\omega^{an}(T)$ is determined by the real part of the phonon self-energy [10,36], which can be phenomenologically expressed by the contribution from three-phonon (3-ph) and four-phonon (4-ph) scattering processes as follows [10]:

$$\Delta\omega^{an}(T) = A\left[1 + 2f_{an}\left(\frac{x}{2}\right)\right] + B\left[1 + 3f_{an}\left(\frac{x}{3}\right) + 3f_{an}^2\left(\frac{x}{3}\right)\right], \quad (3)$$

where $x = \hbar\omega(0)/(k_B T)$, $f_{an}(x) = 1/[\exp(x)-1]$, A and B are fitting constants, and k_B is the Boltzman constant. $f_{an}(x)$ is the Bose-Einstein distribution that describes phonon population at thermal equilibrium. The first and second terms in Eq. (3) correspond to 3-ph and 4-ph scattering processes, respectively. In Eq. (3), the involved phonons can be zone-center or off-center phonons, *e.g.*, the G-mode or D-mode phonons in graphene, respectively. The 3-ph process is simplified as the relaxation of a phonon $\omega_0(\boldsymbol{q}_0)$ into two phonons, $\omega_1(\boldsymbol{q}_1)$ and $\omega_2(\boldsymbol{q}_2)$, where $\boldsymbol{q}_0$, $\boldsymbol{q}_1$ and $\boldsymbol{q}_2$ are the wave vectors of the corresponding phonons. The energy and momentum conservation conditions must be fulfilled in the scattering process, i.e., $\omega_1=\omega_2=\omega_0/2$ and $\boldsymbol{q}_1+\boldsymbol{q}_2=\boldsymbol{q}_0$. Similarly, the second term in Eq. (3) simply describes the decay channel of the phonon $\omega_0(\boldsymbol{q}_0)$ into three phonons, $\omega_1(\boldsymbol{q}_1)$, $\omega_2(\boldsymbol{q}_2)$ and $\omega_3(\boldsymbol{q}_3)$, where $\omega_1=\omega_2=\omega_3=\omega_0/3$ and $\boldsymbol{q}_1+\boldsymbol{q}_2+\boldsymbol{q}_3=\boldsymbol{q}_0$, to fulfill the energy and momentum conservation conditions. Because the total number of involved phonons in the scattering process is three (four), the corresponding anharmonic ph-ph interaction is denoted as 3-ph (4-ph) scattering process. The 3-ph and 4-ph contributions in phenomenological forms of Eq. (3) have been successfully used to well fit *T*-dependent $\Delta\omega$ of silicon [10], diamond [39] and many other materials [40,41].

The terms of $\Delta\omega_G^{TE}$ and $\Delta\omega_G^{an}$ for graphite and graphene can be theoretically calculated using density-functional theory [36], as elucidated in Fig. 3. For both graphene and graphite, the contribution from 4-ph scattering term is dominated in the *T* dependence of $|\Delta\omega_G|$. In addition, the calculated $|\Delta\omega_G^{TE}|$ and $|\Delta\omega_G^{an}|$ (dash-dotted lines in Fig. 3(b)–(e)) in graphene are larger than those in graphite, leading to larger $|\Delta\omega_G|$ in graphene. This is confirmed by the experimental data of S1–S4 in Fig. 3. Indeed, the average $|\Delta\omega_G|$ of S1–S4 at 500 K is about 7.5 cm^{-1}, larger than that (5.5 cm^{-1}) of graphite.

It should be noted that the theoretical 3-ph and 4-ph scattering terms [36] of both graphene and graphite in Fig. 3 can not be fitted by the corresponding 3-ph and 4-ph contributions in phenomenological forms of Eq. (3), respectively. The theoretical 3-ph term makes ω_G blueshift with increasing *T*, although the 3-ph term usually results in redshift of Raman peak with increasing *T* [10,39]. For the experimental results, the deduced *T*-dependent $|\Delta\omega_G^{an}|$ of graphite [7] as well as S1–S4 also can not be fitted by Eq. (3), even the parameter *A* in Eq. (3) is set to be positive. In contrast to the simplified scattering processes in phenomenological forms of Eq. (3), the actual ph-ph decay channels for the E_{2g} mode at Γ point is complicated, as illustrated by Bonini et al. [36]. For instance, in the 3-ph scattering process, the E_{2g} phonon can decay into LA+LA, TA+TA or ZO+ZO phonon pairs with the same frequency under the energy and momentum conservation conditions; moreover, it can also decay into TA+LA phonon pairs with different energies. Importantly, the latter process is dominant. The actual 4-ph scattering process is more complicated. This is why the theoretical $|\Delta\omega_G^{an}|$ and experimentally-reduced one can not be fitted by the simplified 3-ph and 4-ph terms in Eq. (3).

If we directly compare experimental $\Delta\omega_G$ of S1–S4 with the theoretical one including contributions from TE, 3-ph and 4-ph terms, qualitative agreement can be achieved, especially in the temperature range of 4 ~250 K. The small discrepancy in the range of 250 ~500 K may result from a little overestimation of contribution from each term. This is reasonable due to the large discrepancy in TE coefficients of graphene between different groups [35,42,43]. It is also the case for graphite [44,45]. The theoretical $\Delta\omega_G$ of graphite is also in qualitative agreement with the corresponding experimental $\Delta\omega_G$. Note that, S1–S4 are not pristine graphene with $E_F = 0$ eV, but heavily-doped graphenes with E_F ranging from −0.55 eV to −1.05 eV. The qualitative agreement between theoretical $\Delta\omega_G(T)$ of pristine graphene and experimental ones of

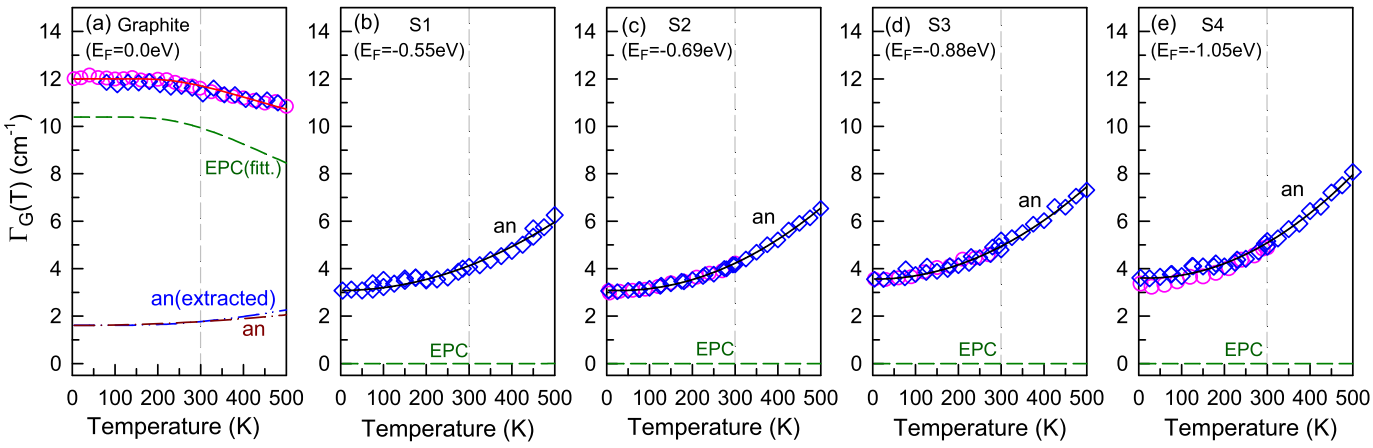

Fig. 4. *T*-dependent Γ_G of (a) graphite [7] and (b–e) S1–S4 excited by 632.8 nm (blue open diamonds) and 514.5 nm (pink open circles). The dark green dashed lines depict the calculated EPC contribution from Eq. (6). In (a), the red solid line represents the total Γ_G of graphite with $E_F = 0$ eV, the dark-red dash-dotted line indicates the corresponding theoretical 3-ph anharmonicity term [36], and the blue dash-dot-dotted line shows the remnant contribution of phonon anharmonicity term extracted from the solid line. In (b)–(e), the dark solid lines are guides to eye to show Γ_G trend with increasing *T*. Note that the system broadening of 1.0 cm^{-1} was subtracted from experimental Γ_G. Vertical gray dashed lines are guides to the eye at room temperature. (A colour version of this figure can be viewed online.)

S1–S4 indicates that $\Delta\omega_G(T)$ is not sensitive to the doping level of graphene, and the frequency change of phonon dispersion in heavily-doped graphene with regard to pristine graphene does not significantly modify the TE effect and ph-ph decay channels.

The *T*-dependent linewidth of a Raman mode is another quantity that provides valuable information on phonon anharmonicity. For a system with zero band gap, phonons can generally decay into lower-energy phonons or by creating an electron-hole pair. Therefore, the corresponding Raman mode has a finite *T*-dependent FWHM, *i.e.*, $\Gamma(T)$, which includes the contribution from phonon anharmonicity (Γ^{an}) and EPC (Γ^{EPC}) corresponds to the above two decay channels [7,36]:

$$\Gamma(T) = \Gamma^{an}(T) + \Gamma^{EPC}(T). \tag{4}$$

By considering the 3-ph and 4-ph scattering processes in the phonon decay channels, Γ^{an} can be phenomenologically expressed as [10]:

$$\Gamma^{an}(T) = C\left[1 + 2f_{an}\left(\frac{x}{2}\right)\right] + D\left[1 + 3f_{an}\left(\frac{x}{3}\right) + 3f_{an}^2\left(\frac{x}{3}\right)\right], \tag{5}$$

where $x = \hbar\omega(0)/(k_B T)$, $\omega(0)$ is the phonon frequency, $f_{an}(x) = 1/(\exp(x) - 1)$, *C* and *D* are fitting constants. This phenomenological form was obtained under the same simple assumption as Eq. (3), of which the optical phonon is assumed to decay into two or three phonons with the same frequency under the energy and momentum conservation conditions, as discussed in Eq. (3). The 3-ph and 4-ph contributions in phenomenological forms of Eq. (5) had also been successfully used to fit *T*-dependent Γ^{an} of silicon [10], SnSe [40] and many other materials [41].

Γ^{EPC} of Eq. (4) is sensitive to the E_F of the system. For doped graphene-based system with zero electron gap, such as graphite and graphene, the Γ^{EPC} term of the G mode (Γ_G^{EPC}) takes the following form [12,36]:

$$\Gamma_G^{EPC}(T) = \Gamma_G^{EPC}(0)\left[f_{epc}\left(\frac{-\hbar\omega_G(0)}{2} - E_F\right) - f_{epc}\left(\frac{\hbar\omega_G(0)}{2} - E_F\right)\right], \tag{6}$$

where $f_{epc}(y) = 1/[\exp(\frac{y}{k_B T}) + 1]$ is the Fermi-Dirac distribution at temperature *T*, and k_B is the Boltzman constant. $\Gamma_G^{EPC}(0) = \frac{\lambda_\Gamma}{4}\omega_G(0)$, in which $\omega_G(0)$ is the phonon frequency of the G mode, λ_Γ is a dimensionless coefficient corresponding to the EPC strength [36] at Γ point. When E_F in doped graphene-based materials is much larger than half of the G mode energy, Γ_G^{EPC} becomes very small and can be neglected.

As shown in Fig. 4(a), $\Gamma_G(T)$ of graphite is completely dominated by the EPC term (dashed line) with $\Gamma_G^{EPC}(0) = 10.4$ cm^{-1} as E_F is 0 eV in graphite. The extracted anharmonic ph-ph interaction term (dash-dot-dotted line) after excluding the contribution from Γ_G^{EPC} is in good agreement with the theoretical one (dash-dotted line) with only 3-ph scattering processes included [36], as depicted in Fig. 4(a). This agreement demonstrates that the 3-ph scattering term is dominant in phonon anharmonicity contributing to $\Gamma_G(T)$ in graphite, which is distinct from the $\Delta\omega_G$ of graphite (Fig. 3(a)) with larger contribution from 4-ph scattering term than that from TE and 3-ph scattering terms.

In contrast to the large Γ_G in graphite (~12 cm^{-1}), S1–S4 show smaller Γ_G at room temperature, only 4 ~5 cm^{-1}, as depicted in Fig. 4(b)–(e). Because E_F of S1–S4 is much larger than $\frac{1}{2}\hbar\omega_G$, the phonon decay channels by creating an electron-hole pair are forbidden due to the Pauli exclusion principle. Therefore, in S1–S4, the EPC term $\Gamma_G^{EPC}(T)$ to Γ_G can be ignored. Indeed, according to E_F of S1–S4, the calculated $\Gamma_G^{EPC}(T)$ by Eq. (6) is equal to 0, as indicated by the dashed lines in Fig. 4(b)–(e). Thus, the observed Γ_G of S1–S4 is only contributed by the anharmonic ph-ph interaction term Γ_G^{an}. The Γ_G^{an} term can not be directly measured in graphite and pristine graphene because of the dominant contribution from Γ_G^{EPC} term. In addition, the experimental Γ_G^{an} of S1–S4 cannot be fitted by the phenomenological form of Eq. (5) even only the 3-ph term is considered, because the decay of E_{2g} phonon into TA + LA phonon pairs is dominant in the anharmonic ph-ph interaction [36] as discussed above.

Similar to the case of graphite, the theoretical calculation shew that Γ_G^{an} of pristine graphene is determined by 3-phonon scattering processes, exhibiting identical *T*-dependence to that of graphite [36]. In general, the lifetime of phonon (τ) is inversely proportional to Γ. In graphene-based materials, the lifetime of the G phonon is associated with both EPC decay process (τ_G^{EPC}) and anahrmonic phonon decay process (τ_G^{an}) [36], *i.e.*, $\tau_G = \tau_G^{EPC} + \tau_G^{an}$. Compared

with the Γ_G of pristine graphene, Γ_G of S1–S4 is determined by the Γ_G^{an} due to the doping-induced Pauli blockage. One can see that the experimental data of Γ_G^{an} in S1–S4 are much larger than the calculated one in pristine graphene [36], indicating much smaller τ_G^{an} of heavily-doped graphene than that of pristine graphene. With increasing E_F from S1 to S4, the corresponding Γ_G^{an} becomes larger and larger at each T as indicated by the experimental data in Fig. 4(b)–(e), implying that the τ_G^{an} in graphene is closely related to its E_F. In consequence, the τ_G^{an} at room temperature decreases in sequence from S1 (~ 1.30 ps) to S4 (~ 1.02 ps), much smaller than that of graphene (~ 1.92 ps) [36,46]. This suggests that the observed decreasing τ_G^{an} with E_F reflects the significant influence of the high carrier density on the anharmonic phonon decay processes. To uncover intrinsic phonon anharmonicity in pristine graphene is still a challenge in experiment because the as-prepared graphene is easily doped by carrier transfer from air molecules and substrate, as discussed by previous work [7].

4. Conclusion

In summary, we have presented a detailed analysis of phonon anharmonicity and EPC in ambient air-stable $FeCl_3$-based stage-1 GICs with different E_F using T-dependent Raman spectroscopy in the range 4~500 K. The $\Delta\omega_G$ shows a nonlinear dependence on temperature, which is well explained by thermal expansion effect and phonon anharmonicity including both 3-ph and 4-ph scattering processes. The similar $\Delta\omega_G(T)$ of heavily-doped graphene with different E_F indicates that the effect of doping on TE effect and ph-ph decay channels can be neglected in graphene. As for the Γ_G in heavily-doped graphene, the monotonous broadening with increasing temperature is rationalized through its dominant ph-ph contribution because the contribution from EPC is prohibited. In particular, the intrinsic contribution from phonon anharmonicity in heavily-doped graphene is measured, which is dependent on the E_F and decreases as the E_F approaches to the Dirac point. Since phonon anharmonicity and EPC are critical in thermal response processes, this work is helpful for understanding and controlling thermal and electronic transport in graphene-related materials, such as carbon nanotubes and twisted graphene.

CRediT authorship contribution statement

X. Chen: performed experiments, prepared the samples, Data curation, Formal analysis, Writing – original draft. **M.-L. Lin:** Data curation, Formal analysis, Writing – original draft. **X. Cong:** Data curation, Formal analysis. **Y.-C. Leng:** prepared the samples. **X. Zhang:** Formal analysis. **P.-H. Tan:** Conceptualization, Project administration, Supervision, Data curation, Formal analysis, Writing – original draft.

Declaration of competing interest

The authors declare that they have no known competing financial interests or personal relationships that could have appeared to influence the work reported in this paper.

Acknowledgments

We acknowledge support from the National Key Research and Development Program of China (Grant No. 2016YFA0301204), the National Natural Science Foundation of China (Grant Nos. 12004377 and 11874350), CAS Key Research Program of Frontier Sciences (Grant Nos. ZDBS-LY-SLH004 and XDPB22) and the project funded by China Postdoctoral Science Foundation (Grant No. 2019TQ0317).

References

[1] S. Ghosh, I. Calizo, D. Teweldebrhan, E.P. Pokatilov, D.L. Nika, A.A. Balandin, et al., Extremely high thermal conductivity of graphene: prospects for thermal management applications in nanoelectronic circuits, Appl. Phys. Lett. 92 (2008), 151911, https://doi.org/10.1063/1.2907977.
[2] A.A. Balandin, S. Ghosh, W. Bao, I. Calizo, D. Teweldebrhan, F. Miao, et al., Superior thermal conductivity of single-layer graphene, Nano Lett. 8 (3) (2008) 902–907, https://doi.org/10.1021/nl0731872.
[3] D.H. Chae, B. Krauss, K. von Klitzing, J.H. Smet, Hot phonons in an electrically biased graphene constriction, Nano Lett. 10 (2) (2010) 466–471, https://doi.org/10.1021/nl903167f.
[4] K. Gao, R. Dai, Z. Zhang, Z. Ding, Anharmonic effects in single-walled carbon nanotubes, J. Phys. Condens. Matter 19 (48) (2007), 486210, https://doi.org/10.1088/0953-8984/19/48/486210.
[5] I. Calizo, A.A. Balandin, W. Bao, F. Miao, C.N. Lau, Temperature dependence of the Raman spectra of graphene and graphene multilayers, Nano Lett. 7 (9) (2007) 2645–2649, https://doi.org/10.1021/nl071033g.
[6] J. Lin, L. Guo, Q. Huang, Y. Jia, L. Kang, X. Lai, et al., Anharmonic phonon effects in Raman spectra of unsupported vertical graphene sheets, Phys. Rev. B 83 (12) (2011) 1161–1171, https://doi.org/10.1103/PhysRevB.83.125430.
[7] H.N. Liu, X. Cong, M.L. Lin, P.H. Tan, The intrinsic temperature-dependent Raman spectra of graphite in the temperature range from 4 K to 1000 K, Carbon 152 (2019) 451–458, https://doi.org/10.1016/j.carbon.2019.05.016.
[8] M. Lazzeri, F. Mauri, Nonadiabatic Kohn anomaly in a doped graphene monolayer, Phys. Rev. Lett. 97 (2006), 266407, https://doi.org/10.1103/PhysRevLett.97.266407.
[9] M. Lazzeri, M. Calandra, F. Mauri, Anharmonic phonon frequency shift in MgB_2, Phys. Rev. B 68 (2003), 220509, https://doi.org/10.1103/PhysRevB.68.220509.
[10] M. Balkanski, R. Wallis, E. Haro, Anharmonic effects in light scattering due to optical phonons in silicon, Phys. Rev. B 28 (4) (1983) 1928, https://doi.org/10.1103/PhysRevB.28.1928.
[11] S. Piscanec, M. Lazzeri, F. Mauri, A. Ferrari, J. Robertson, Kohn anomalies and electron-phonon interactions in graphite, Phys. Rev. Lett. 93 (18) (2004), 185503, https://doi.org/10.1103/PhysRevLett.93.185503.
[12] S. Pisana, M. Lazzeri, C. Casiraghi, K.S. Novoselov, A.K. Geim, A.C. Ferrari, et al., Breakdown of the adiabatic Born-Oppenheimer approximation in graphene, Nat. Mater. 6 (3) (2007) 198–201, https://doi.org/10.1038/nmat1846.
[13] J. Yan, Y. Zhang, P. Kim, A. Pinczuk, Electric field effect tuning of electron-phonon coupling in graphene, Phys. Rev. Lett. 98 (2007), 166802, https://doi.org/10.1103/PhysRevLett.98.166802.
[14] K.T. Nguyen, D. Abdula, C.L. Tsai, M. Shim, Temperature and gate voltage dependent Raman spectra of single-layer graphene, ACS Nano 5 (6) (2011) 5273–5279, https://doi.org/10.1021/nn201580z.
[15] I. Efthimiopoulos, S. Mayanna, E. Stavrou, A. Torode, Y. Wang, Extracting the anharmonic properties of the G-band in graphene nanoplatelets, J. Phys. Chem. C 124 (8) (2020) 4835–4842, https://doi.org/10.1021/acs.jpcc.9b10875.
[16] G. Montagnac, R. Caracas, E. Bobocioiu, F. Vittoz, B. Reynard, Anharmonicity of graphite from UV Raman spectroscopy to 2700 K, Carbon 54 (2013) 68–75, https://doi.org/10.1016/j.carbon.2012.11.004.
[17] E.A. Kolesov, M.S. Tivanov, O.V. Korolik, O.O. Kapitanova, H.D. Cho, T.W. Kang, et al., Phonon anharmonicities in supported graphene, Carbon 141 (2019) 190–197, https://doi.org/10.1016/j.carbon.2018.09.020.
[18] N. Jung, N. Kim, S. Jockusch, N.J. Turro, P. Kim, L. Brus, Charge transfer chemical doping of few layer graphenes: charge distribution and band gap formation, Nano Lett. 9 (12) (2009) 4133–4137, https://doi.org/10.1021/nl902362q.
[19] W.J. Zhao, P.H. Tan, J. Liu, A.C. Ferrari, Intercalation of few-layer graphite flakes with $FeCl_3$: Raman determination of fermi level, layer by layer decoupling, and stability, J. Am. Chem. Soc. 133 (15) (2011) 5941–5946, https://doi.org/10.1021/ja110939a.
[20] M. Kalbac, A. Reina-Cecco, H. Farhat, J. Kong, L. Kavan, M.S. Dresselhaus, The influence of strong electron and hole doping on the Raman intensity of chemical vapor-deposition graphene, ACS Nano 4 (10) (2010) 6055–6063, https://doi.org/10.1021/nn1010914.
[21] M.S. Dresselhaus, G. Dresselhaus, Intercalation compounds of graphite, Adv. Phys. 51 (1) (2002) 1–186, https://doi.org/10.1080/00018730110113644.
[22] N. Emery, C. Hérold, M. d'Astuto, V. Garcia, C. Bellin, J.F. Marêché, et al., Superconductivity of bulk CaC_6, Phys. Rev. Lett. 95 (2005), 087003, https://doi.org/10.1103/PhysRevLett.95.087003.
[23] N. Kim, K.S. Kim, N. Jung, L. Brus, P. Kim, Synthesis and electrical characterization of magnetic bilayer graphene intercalate, Nano Lett. 11 (2) (2011) 860–865, https://doi.org/10.1021/nl104228f.
[24] I. Khrapach, F. Withers, T.H. Bointon, D.K. Polyushkin, W.L. Barnes, S. Russo, et al., Novel highly conductive and transparent graphene-based conductors, Adv. Mater. 24 (21) (2012) 2844–2849, https://doi.org/10.1002/adma.201200489.
[25] D. Zhan, L. Sun, Z.H. Ni, L. Liu, X.F. Fan, Y. Wang, et al., $FeCl_3$-based few-layer graphene intercalation compounds: single linear dispersion electronic band structure and strong charge transfer doping, Adv. Funct. Mater. 20 (20) (2010) 3504–3509, https://doi.org/10.1002/adfm.201000641.
[26] K.S. Novoselov, A.K. Geim, S.V. Morozov, D. Jiang, Y. Zhang, S.V. Dubonos, et al., Electric field effect in atomically thin carbon films, Science 306 (5696) (2004) 666–669, https://doi.org/10.1126/science.1102896.
[27] W.J. Zhao, P.H. Tan, J. Zhang, J. Liu, Charge transfer and optical phonon mixing

in few-layer graphene chemically doped with sulfuric acid, Phys. Rev. B 82 (2010), 245423, https://doi.org/10.1103/PhysRevB.82.245423.
[28] D.S. Smith, P.C. Eklund, Optical reflectance studies of stage 1-6 graphite-$FeCl_3$ intercalation compounds, MRS Proc. 20 (1982) 99, https://doi.org/10.1557/PROC-20-99.
[29] A. Das, S. Pisana, B. Chakraborty, S. Piscanec, S. Saha, U. Waghmare, et al., Monitoring dopants by Raman scattering in an electrochemically top-gated graphene transistor, Nat. Nanotechnol. 3 (4) (2008) 210–215, https://doi.org/10.1038/nnano.2008.67.
[30] J.B. Wu, M.L. Lin, X. Cong, H.N. Liu, P.H. Tan, Raman spectroscopy of graphene-based materials and its applications in related devices, Chem. Soc. Rev. 47 (2018) 1822–1873, https://doi.org/10.1039/C6CS00915H.
[31] L. Pietronero, S. Strässler, Bond-length change as a tool to determine charge transfer and electron-phonon coupling in graphite intercalation compounds, Phys. Rev. Lett. 47 (1981) 593–596, https://doi.org/10.1103/PhysRevLett.47.593.
[32] A. Das, B. Chakraborty, S. Piscanec, S. Pisana, A.K. Sood, A.C. Ferrari, Phonon renormalization in doped bilayer graphene, Phys. Rev. B 79 (2009), 155417, https://doi.org/10.1103/PhysRevB.79.155417.
[33] S. Piscanec, M. Lazzeri, F. Mauri, A.C. Ferrari, J. Robertson, Kohn anomalies and electron-phonon interactions in graphite, Phys. Rev. Lett. 93 (2004), 185503, https://doi.org/10.1103/PhysRevLett.93.185503.
[34] C.F. Chen, C.H. Park, B.W. Boudouris, J. Horng, B. Geng, C. Girit, et al., Controlling inelastic light scattering quantum pathways in graphene, Nature 471 (2011) 617, https://doi.org/10.1038/nature09866.
[35] S. Tian, Y. Yang, Z. Liu, C. Wang, R. Pan, C. Gu, et al., Temperature-dependent Raman investigation on suspended graphene: contribution from thermal expansion coefficient mismatch between graphene and substrate, Carbon 104 (2016) 27–32, https://doi.org/10.1016/j.carbon.2016.03.046.
[36] N. Bonini, M. Lazzeri, N. Marzari, F. Mauri, Phonon anharmonicities in graphite and graphene, Phys. Rev. Lett. 99 (17) (2007), 176802, https://doi.org/10.1103/PhysRevLett.99.176802.
[37] J. Menéndez, M. Cardona, Temperature dependence of the first-order Raman scattering by phonons in Si, Ge, and α-Sn: anharmonic effects, Phys. Rev. B 29 (4) (1984) 2051, https://doi.org/10.1103/PhysRevB.29.2051.
[38] P.H. Tan, Y. Deng, Q. Zhao, W. Cheng, The intrinsic temperature effect of the Raman spectra of graphite, Appl. Phys. Lett. 74 (13) (1999) 1818, https://doi.org/10.1063/1.123096.
[39] J.B. Cui, K. Amtmann, J. Ristein, L. Ley, Noncontact temperature measurements of diamond by Raman scattering spectroscopy, J. Appl. Phys. 83 (12) (1998) 7929–7933, https://doi.org/10.1063/1.367972.
[40] F. Liu, P. Parajuli, R. Rao, P.C. Wei, A. Karunarathne, S. Bhattacharya, et al., Phonon anharmonicity in single-crystalline SnSe, Phys. Rev. B 98 (2018), 224309, https://doi.org/10.1103/PhysRevB.98.224309.
[41] Y.K. Peng, Z.Y. Cao, L.C. Chen, N. Dai, Y. Sun, X.J. Chen, Phonon anharmonicity of tungsten disulfide, J. Phys. Chem. C 123 (41) (2019) 25509–25514, https://doi.org/10.1021/acs.jpcc.9b07553.
[42] D. Yoon, Y.W. Son, H. Cheong, Negative thermal expansion coefficient of graphene measured by Raman spectroscopy, Nano Lett. 11 (8) (2011) 3227–3231, https://doi.org/10.1021/nl201488g.
[43] S. Linas, Y. Magnin, B. Poinsot, O. Boisron, G.D. Förster, V. Martinez, et al., Interplay between Raman shift and thermal expansion in graphene: temperature-dependent measurements and analysis of substrate corrections, Phys. Rev. B 91 (2015), 075426, https://doi.org/10.1103/PhysRevB.91.075426.
[44] N. Mounet, N. Marzari, First-principles determination of the structural, vibrational and thermodynamic properties of diamond, graphite, and derivatives, Phys. Rev. B 71 (2005), 205214, https://doi.org/10.1103/PhysRevB.71.205214.
[45] M.A. Abdullah, T.M.B. Albarody, A.R. Hussein, Graphite thermal expansion coefficient measured by in-situ X-ray diffraction, Nanotechnology 31 (28) (2020), 285709, https://doi.org/10.1088/1361-6528/ab8040.
[46] I. Chatzakis, H. Yan, D. Song, S. Berciaud, T.F. Heinz, Temperature dependence of the anharmonic decay of optical phonons in carbon nanotubes and graphite, Phys. Rev. B 83 (2011), 205411, https://doi.org/10.1103/PhysRevB.83.205411.